



# Model tests on resistance and seakeeping performance of wave-piercing high-speed vessel with spray rails

Jeonghwa Seo<sup>a</sup>, Hak-Kyu Choi<sup>a</sup>, Uh-Cheul Jeong<sup>b</sup>, Dong Kun Lee<sup>c</sup>, Shin Hyung Rhee<sup>a,d</sup>,  
Chul-Min Jung<sup>e</sup>, Jaehoon Yoo<sup>f,\*</sup>

<sup>a</sup> Dept. of Naval Architecture and Ocean Engineering, Seoul National University, Seoul, South Korea

<sup>b</sup> Dept. of Naval Architecture and Ocean Engineering, Inha Technical College, Incheon, South Korea

<sup>c</sup> Dept. of Naval Architecture and Ocean Engineering, Mokpo National Maritime University, Mokpo, South Korea

<sup>d</sup> Research Institute of Marine Systems Engineering, Seoul National University, Seoul, South Korea

<sup>e</sup> The 6th R&D Institute-3rd Directorate, Agency for Defense Development, Changwon, South Korea

<sup>f</sup> Dept. of Ocean Engineering, Mokpo National University, Muan, South Korea

Received 3 February 2016; revised 18 May 2016; accepted 22 May 2016

Available online 16 July 2016

## Abstract

The resistance and seakeeping performance of a high-speed monohull vessel were investigated through a series of model tests in a towing tank. The hull had a slender wave-piercing bow, round bilge, and small deadrise angle on stern. Tests on the bare hull in calm water were first conducted and tests on spray rails followed. The spray rails were designed to control the flow direction and induce a hydrodynamic lift force on the hull bottom to reduce trim angle and increase rise of the hull. The maximum trim of the bare hull was  $4.65^\circ$  at the designed speed, but the spray rails at optimum location reduced trim by  $0.97^\circ$ . The ship motion in head seas was examined after the calm water tests. Attaching the rails on the optimum location effectively reduced the pitch and heave motion responses. The vertical acceleration at the fore perpendicular reduced by 11.3%. The effective power in full scale was extrapolated from the model test results and it was revealed that the spray rails did not have any negative effects on the resistance performance of the hull, while they effectively stabilized the vessel in calm water and waves.

Copyright © 2016 Society of Naval Architects of Korea. Production and hosting by Elsevier B.V. This is an open access article under the CC BY-NC-ND license (<http://creativecommons.org/licenses/by-nc-nd/4.0/>).

**Keywords:** Wave-piercing bow; High-speed vessel; Model test; Seakeeping

## 1. Introduction

High-speed vessels are designed to reach a relatively high speed with limited motor power. Therefore, various hull designs and appendages have been applied to reduce the wave-making resistance and the wetted surface area. Among them, the planing hull is one of the most widely used. This planing hull is designed to reduce the drag force by raising the hull,

utilizing the hydrodynamic pressure at the bottom of the ship. As the hull is not equipped with prominent appendages such as hydrofoils, the hull shape is relatively simple; design, manufacturing, and maintenance of the planing hull are easier than those of other types of high speed vessels. The planing hull employs a wide bottom area to obtain sufficient lift force to raise the hull; thus, strong resonances in pitch and heave motions develop periodically in response to waves because of the wide bottom. Because strong vertical resonance motion and the slamming impact can damage the hull and harm passengers, it is important in the design stage of the planing hull to analyze and minimize the impact of the hull in waves.

\* Corresponding author.

E-mail address: [yoojaehoon@mokpo.ac.kr](mailto:yoojaehoon@mokpo.ac.kr) (J. Yoo).

Peer review under responsibility of Society of Naval Architects of Korea.

**List of symbols**

$A$	Wave amplitude $A = H/2$ (m)
$B$	Maximum Breadth of the ship (m)
$C_R$	Residual resistance coefficient
$Fr_V$	Volumetric Froude number $Fr = V_A/\sqrt{GV^{\frac{1}{3}}}$
$G$	Gravitational acceleration (9.8 m/s <sup>2</sup> )
$H$	Wave height (m)
$k$	Wave number $k = 2\pi/\lambda$
$L_{PP}$	Length between perpendiculars (m)
$Rn$	Reynolds number based on the length between perpendiculars $Rn = \rho L_{PP} V_A / \mu$
$T$	Draft of the ship (m)
$V_A$	Ship advance speed (m/s)
$\nabla$	Ship displacement (m <sup>3</sup> )
$\lambda$	Wave length (m)
$\mu$	Dynamic viscosity of water (kg/m·s)
$\rho$	Density of water (kg/m <sup>3</sup> )

Grigoropoulos and Chalkias (2010) used the Rankine source panel method to analyze the motion of a planing craft in waves. They developed a method to estimate the vertical acceleration of the bow and proposed an improved design of a double-chine planing hull. The modified hull was more prismatic than the original and the vertical acceleration of the bow in waves was reduced by 25.9%. Sun and Faltinsen (2011) used the boundary element method to analyze the planing hull motion in waves and the vertical acceleration of the bow with wave condition variations. The analysis method was applied to various speeds and loading conditions; these researchers reported that the magnitude of the sharp vertical acceleration peaks at the resonant wave encounter frequency ranged from 2  $G$  to 7  $G$ , according to the ship configuration variations.

In addition to the above numerical approaches, studies on the seakeeping performance of the planing hull were also implemented through model tests. Kim et al. (2013) conducted model tests for three different types of planing hull designs in calm water and in head seas to measure and compare the bow vertical acceleration. They found that the vertical acceleration of the bow and the motion response to waves could be reduced by applying the wave-piercing bow design. Begovic et al. (2014) performed seakeeping model tests of planing hull designs with various deadrise angles, and they reported a decrease in the vertical acceleration of the bow by introducing large deadrise angle to the hull bottom.

Dynamic stability of planing hull is an important topic in design, as well as vertical acceleration of the bow. Previous experimental and mathematical studies on transversal stability have reported that transversal stability of planing hulls is very sensitive to their bottom design and attitude in planing (Lewandowski, 1997; Katayama et al., 2007). To insure suitable dynamic stability and maneuverability, small deadrise angle is recommended, but it results in increasing vertical

acceleration of the bow, as described above. It is hard to satisfy both of seakeeping and maneuverability of planing hull, thus a different hull shape has been developed and tested to overcome the limitations of planing hulls design.

A slender hull with wave-piercing bow has been suggested as an alternative. Wave-piercing bow was shaped like a sharp axe blade, to provide small displacement on the bow (Kim et al., 2013). Thus, the displacement of the ship is concentrated near the stern; the Center of Gravity (CG) is also located near the stern. Previous studies on wave-piercing bow have revealed that this configuration reduces motion and added resistance of the hull in waves.

Keuning et al. (2001) applied a wave-piercing bow to a fast patrol boat and analyzed its motion in waves by applying the non-linear strip theory. The results were compared with those for the original hull to indicate that the hull with a wave-piercing bow reduced the vertical acceleration of the bow. Moreover, it was reported that the application of the wave-piercing bow resulted in the decrease of the trim in running (Keuning et al., 2002).

When a wave-piercing bow is used in a high-speed vessel, the breath of the bow decreases;  $L_{PP}/B$  of the ship increases and the transverse stability reduced in wave-piercing vessels. Hence, the wave-piercing bow has been mainly applied to catamarans, which have good transversal stability. By introducing wave-piercing bow to a catamaran, it was reported that the slamming impacts of the bow diminishes (Lavroff et al., 2013).

Herein, a high-speed monohull with a wave-piercing bow was designed and tested to assess its resistance and seakeeping performance. As its design principle was different from that of planing hulls, which have been used for high speed vessels most frequently, the resistance and seakeeping characteristics were expected to be dissimilar to those of planing hulls. Moreover, spray rails with location variations were also tested in calm water and head seas conditions. Appendages similar to spray rails in this study have been applied to planing hulls to reduce trim in running and longitudinal and transverse stability (Yousefi et al., 2013; Larsson et al., 2014). As the optimal location of spray rails varies with the hull geometry and flow stagnation line (Clement, 1964), spray rails with various locations were tested in calm water first, and the optimal spray rails which minimize the running trim and resistance at the design speed were chosen. The hull with optimal spray rails were also tested in head seas. These model test results provided estimates of the vertical acceleration of the bow and its full-scale effective power in head seas.

This paper is organized as follows. The next section explains the experimental model, facility, measurement system, and conditions. The following section details the experimental results and discussion, wherein the first subsection covers the resistance test results in calm water for the bare hull and spray rails and the second subsection describes the seakeeping test results in head seas. The last section summarizes the conclusions and future work of this study.

## 2. Experimental methods and conditions

### 2.1. Testing facility and measurement systems

The model tests were conducted in the Seoul National University Towing Tank (SNUTT). The length, width, and depth of the towing tank were 110 m, 8 m, and 3.5 m, respectively. In the towing tank, a truss-type high-speed carriage was installed to tow the test model. Fig. 1 presents a schematic diagram of the towing system. It was installed on the high-speed towing carriage and allowed test model motions with two degrees of freedom, in pitch and heave. The specific design and mechanisms of the gimbal were detailed in the experimental study by Kim (2012). The gimbal was designed to transmit the external towing force from the towing carriage to the test model in the longitudinal direction of the hull, regardless of the running trim. The pivot of the gimbal, *i.e.*, the center of pitch motion, was located at the intersection of the propulsor axis and the vertical CG of the model ship.

The heave and pitch motions of the model were independently measured by two potentiometers. A load cell with full-bridge strain gauges was used to measure the resistance force of the model. The maximum measurable force in the longitudinal direction was 200 N. The resistance force and the pitch and heave motions were measured using a data acquisition system (MX840A, Hottinger Baldwin Messtechnik GmbH, Darmstadt, Germany) with a sampling frequency of 100 Hz.

The test system constrained roll and yaw motion to focus on pitch and heave motion, which are primarily induced in head seas. As mentioned in the introduction, wave-piercing hulls have less static transversal stability than planing hulls, due to slender hull geometry. In the case of dynamic stability, on the other hand, attitude changes in running wave-piercing hulls are similar to those in semi-displacement type hulls and smaller than those in planing hull, thus changes in dynamic stability of wave-piercing hull is expected to be small. The transverse stability can be examined by towing tests with free-roll (Katayama et al., 2007), but the experimental setup was not applied in this study, thus measuring roll motion or moment in towing is remained as future work.

The measurement system's test uncertainty was assessed following the standard of the American Society of Mechanical Engineers (ASME, 2005). Table 1 shows uncertainty

assessment results. The total uncertainties with 95% confidence level of the pitch angle, heave displacement, and resistance were 0.0630°, 1.14 mm, and 0.572 N, respectively. Dynamic range means maximum of measured value in calm water towing test.

### 2.2. Test model

The test model was a monohull with a wave-piercing bow. Fig. 2 shows the geometry of the model ship. While previous studies on wave-piercing hull have focused on the installation of wave-piercing bow to existing high speed hulls to examine bow modification effects (Keuning et al., 2002; Kim et al., 2013), the newly-designed wave-piercing monohull had different hull geometry from traditional planing hull. The design principle of wave-piercing hull was maintaining small trim angle to immerse the bow edge in waves, rather than generate lift force on the hull bottom; thus, hard chine was excluded in the hull design initially.

The wave-piercing bow was designed to reduce vertical motion in head seas, by reducing the volume of the bow; the bow was deep-V shaped and very slender, thus displacement was concentrated near the stern with small deadrise angle. The deadrise angle of the test model was 15° at aft perpendicular (AP). It is reported that small deadrise angle increases vertical acceleration of the bow in waves, but the wave-piercing bow could reduce the bow acceleration effectively. After the tests of bare hull with round bilge, spray rails with installation location variation were applied, to confirm resistance performance improvements and provide transverse stability.

Like other high speed vessels, trim tabs or interceptors were able to be applied to the hull; but spray rails which could passively provide additional roll stability were considered first in the study, as the wave-piercing monohull has inferior transverse stability because of large  $L_{PP}/B$ . Moreover, trim in running was small enough as designed, thus appendages for reducing trim, *i.e.*, interceptors or trim tabs, were not necessary. Future study will concern effects of spray rails on transverse stability.

$L_{PP}$  and displacement of the ship in full scale were 30 m and 59.8 m<sup>3</sup>, respectively. The maximum design speed of the vessel in full scale was 50 knots. The scale ratio of the test model was 1/15 and the  $L_{PP}$  of the test model was 2 m. Principal particulars of the hull are presented in Table 2. As the bow was slender and had a small displacement, the CG of the ship was located at 32.8% of  $L_{PB}$  forward from AP.

The bare hull with round bilge was tested first, and spray rails were attached on the hull to reduce trim in running. They were designed to change the flow direction on the hull bottom and provide additional lift force on the stern. The rails were placed from the longitudinal CG of the hull to AP. They were parallel to the longitudinal centerline of the hull. They were positioned at various vertical locations to find the optimal location, where the trim in running was minimized. Fig. 3 shows the location and geometry of spray rails. The fore

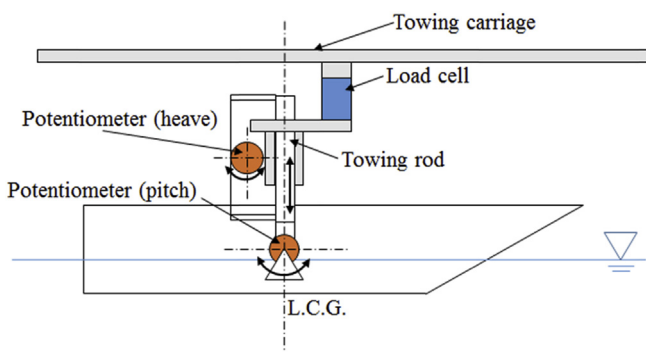


Fig. 1. Schematic diagram of the towing mechanisms.

Table 1  
Test uncertainty.

Item	Unit	Systematic error	Random error	Total uncertainty (95% confidence level)	Dynamic range	Total uncertainty/Dynamic range (%)
Towing speed	<i>m/s</i>	0.0314	0.0025	0.0630	7.969	0.791
Trim angle	°	0.05	0.042	0.131	4.65	2.81
Rise of C.G.	<i>mm</i>	0.25	0.513	1.14	53.8	2.12
Resistance	<i>N</i>	0.032	0.284	0.572	40.47	1.41
Wave period	<i>s</i>	0.005	0.000100	0.0100	2.53	0.395
Wave height	<i>mm</i>	0.05	0.178	0.370	66.6	0.555

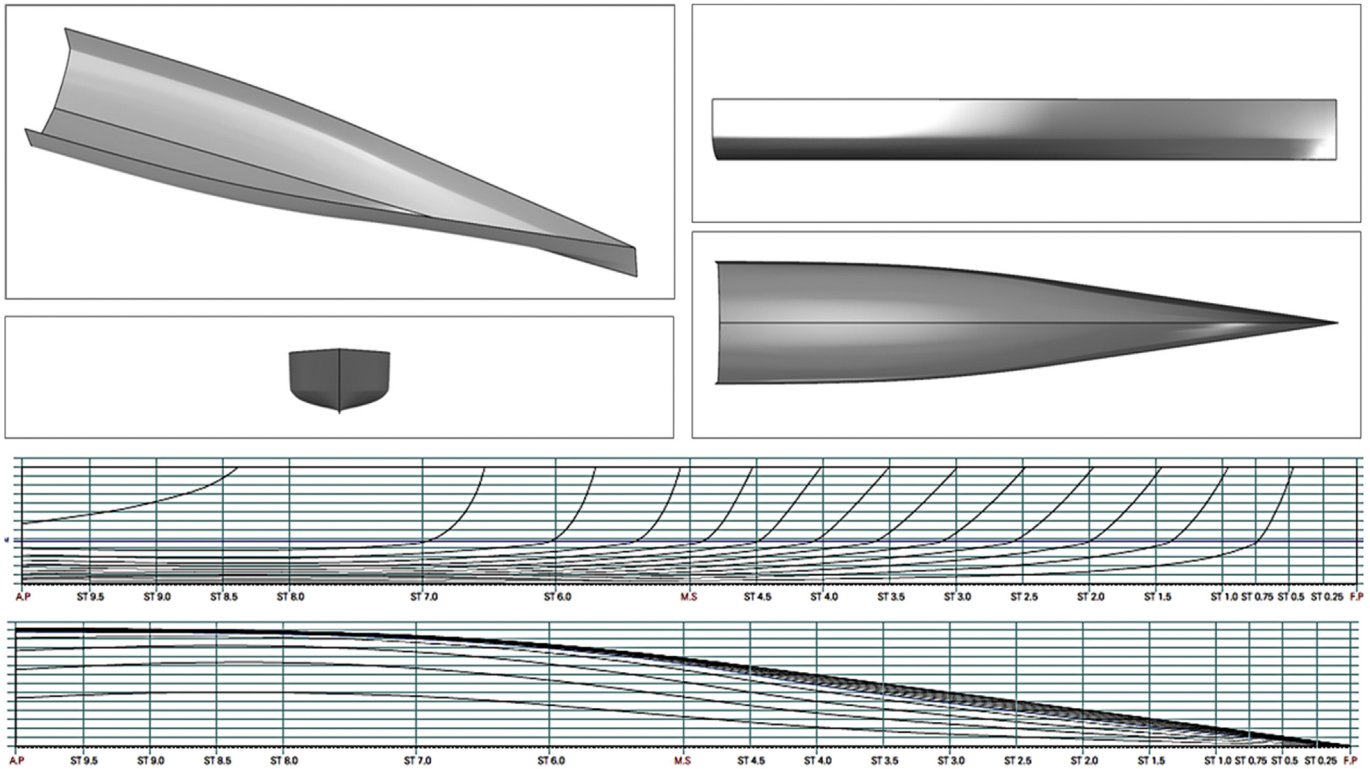


Fig. 2. The wave-piercing monohull: the geometry of the hull (top) and lines of the hull (bottom).

Table 2  
Principal particulars of the wave piercing monohull.

Item	Unit	Full scale	Test model
Scale ratio		1	1/15
$L_{PP}$	<i>m</i>	30	2.0
$B$	<i>m</i>	5.12	0.341
$T$	<i>m</i>	0.93	0.062
Water plane area	$m^2$	95.9	0.426
Wetted surface area	$m^2$	119.0	0.528
$\nabla$	$m^3$	59.8	0.0177
Longitudinal center of buoyancy (from the aft perpendicular)	<i>m</i>	9.87	0.658
Vertical center of buoyancy (from the baseline)	<i>m</i>	0.576	0.0384
Vertical center of gravity (from the baseline)	<i>m</i>	1.61	0.107
GM	<i>m</i>	1.53	0.102
Radius of gyration (transversal direction)	<i>m</i>	7.5	0.50
Block coefficient		0.408	

part of the rails was tapered to make the surface smooth. In the model tests, the distance from the bottom of the rails to the calm water surface were chosen at 8%, 24%, and 40% of  $T$ . Its width was 22.5% of  $T$ .

### 2.3. Test conditions

Model tests were first conducted in calm water conditions (Table 3).  $Fr_v$  herein ranged from 0.416 to 4.158. Corresponding ship speed in the full scale ranged from 5 to 50 *knots*. During towing, trim, rise of CG, and resistance were measured. Bare hull and three spray rail cases were tested.

In head seas condition, bare hull and a spray rail (24%  $T$ ) case were tested. Table 4 shows the wave conditions for the tests in head seas.  $\lambda/L_{PP}$  ranged from 1.0 to 5.0. Test model in head seas was towed in constant speed, which implies thrust variation in the full scale trial. The model tests of the bare hull

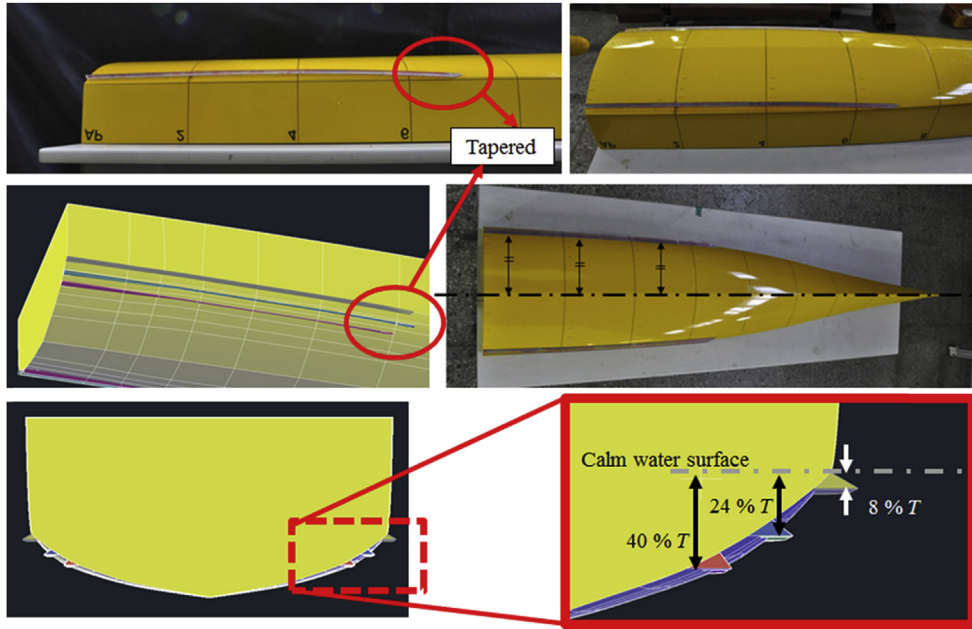


Fig. 3. The location and geometry of spray rails.

Table 3  
Test conditions in calm water.

$Fr_v$	Full scale		Model scale	
	$V_A$ (knots)	$Rn$	$V_A$ (m/s)	$Rn$
0.416	5	66,000,000	0.66	1,144,000
0.832	10	133,000,000	1.33	2,289,000
1.247	15	199,000,000	1.99	3,434,000
1.663	20	266,000,000	2.66	4,579,000
2.079	25	332,000,000	3.32	5,724,000
2.495	30	399,000,000	3.98	6,869,000
2.910	35	465,000,000	4.65	8,014,000
3.326	40	532,000,000	5.31	9,159,000
3.742	45	598,000,000	5.98	10,304,000
4.158	50	665,000,000	6.64	11,449,000

in waves were conducted at  $Fr_v$  of 2.495 (3.98 m/s in model scale) only, which corresponds to 30 knots in the full scale. Finally, tests of the appended hull with 24% of  $T$  spray rail were performed under 2.66, 3.98, and 5.31 m/s, which correspond to 20, 30, and 40 knots in the full scale, respectively.

Table 4  
Wave conditions of tests in head seas.

$\lambda/L_{PP}$	Full scale					Model scale	
	$\lambda$ (m)	Wave frequency (rad/s)	Wave encounter frequency (rad/s)			$\lambda$ (m)	Wave frequency (rad/s)
			20 knots	30 knots	40 knots		
1.0	30	1.43	2.61	3.32	4.04	2.0	5.56
1.5	45	1.17	1.91	2.39	2.87	3.0	4.52
2.0	60	1.01	1.54	1.90	2.26	4.0	3.93
2.5	75	0.906	1.31	1.60	1.89	5.0	3.51
3.0	90	0.827	1.15	1.39	1.63	6.0	3.20
4.0	120	0.716	0.944	1.12	1.30	8.0	2.78
5.0	150	0.640	0.810	0.954	1.10	10.0	2.48

### 3. Results and discussion

#### 3.1. Resistance tests in calm water

Fig. 4 shows snapshots of the bare hull resistance tests. The trim increased at high speed conditions. For  $Fr_v$  above 3.326, which corresponds to 40 knots in full scale, the bow protruded from the water surface due to excessive trim, and the bottom of the bow, rather than the sharp bow edge, touched the water surface and it resulted in water spray around the hull.

The trim, CG rise, and resistance measurement results in calm water are shown in Fig. 5. The observed changes in the trim of the wave-piercing monohull differed from those of the conventional planing hulls. Generally, a planing hull exhibits a rapid increase of trim at low  $Fr_v$  and the trim gradually decreases in high speed range where sufficient lift force is produced and the hull planes. In the case of the present wave-piercing monohull, however, trim increased as the ship's speed increased, and the trim converged to  $4.6^\circ$  in the maximum design speed condition. Furthermore, the CG rise

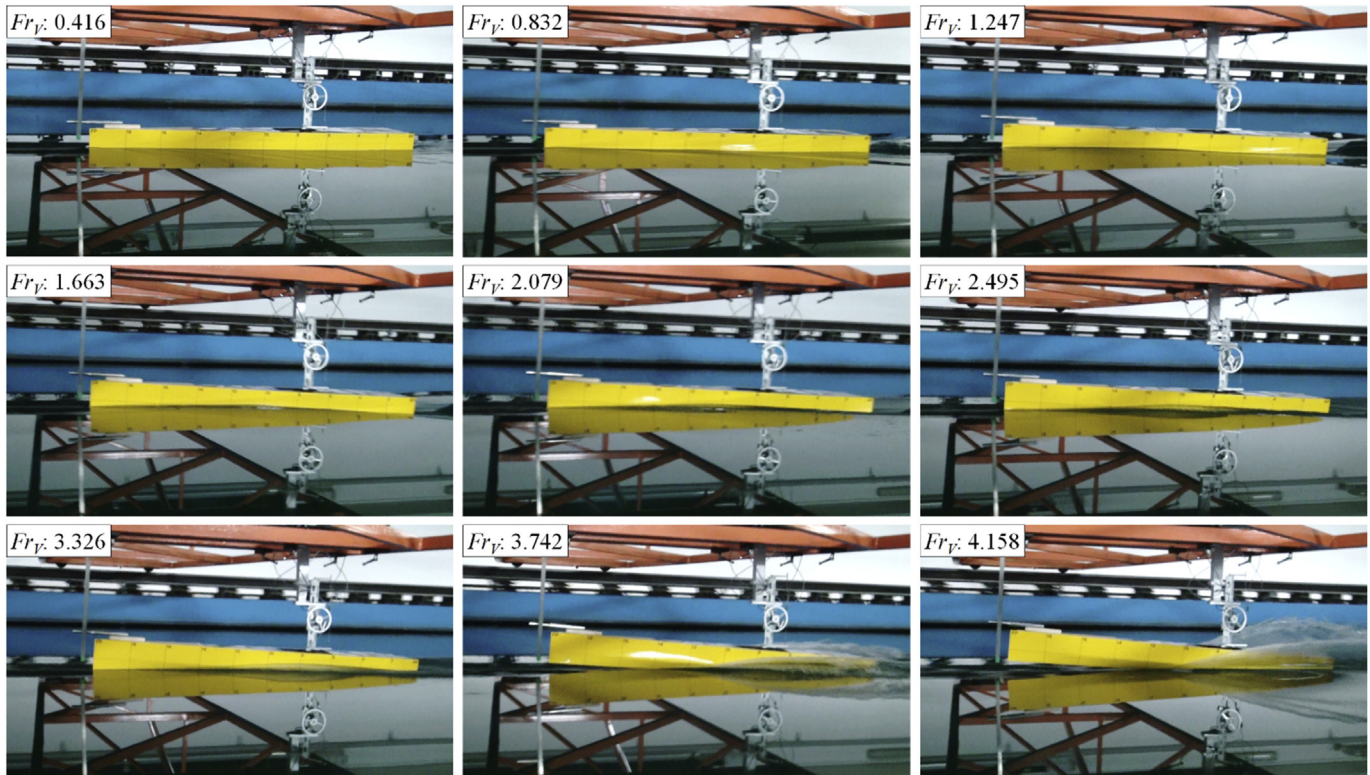


Fig. 4. Snapshots of the resistance tests in bare hull condition in calm water.

was negative for  $Fr_v$  less than 2.079, whereas it increased to 38 mm in the design speed. This change in trim and CG rise was similar to the results for the wave-piercing hull provided by Keuning et al. (2002) and the experimental results for the wave-piercing semi-displacement-type vessel by Kim (2012).

The spray rails were designed to increase the lift force around the stern; thus, the stern rose and the trim reduced, as the center of pressure on the hull bottom moved toward the stern and the pressure magnitude increased. The ship speed where the spray rails function effectively increased as the rails were placed deeper. As the ship's speed increased, the hull rose and the rails became closer to the water surface. This implies that the spray rails effectively controlled the flow and suppress the water spray when they are located near the water surface and stagnation point, as reported in previous study (Clement, 1964).

The hull had round bilge and smooth bottom without hard chine, thus CG rise in high speed was relatively smaller than planing hulls; but it was confirmed that spray rails worked like hard chine of planing hulls and increased CG rise if they were located properly. Considering the operation speed range of the ship, the rails installed at 24% of  $T$  exhibited the best trim control performance. When these rails were applied, the resistance decreased by 6.28% and the CG rise increased by 40.1% at the design speed.

As the high-speed hull rose during running in high speed, the wetted surface area decreased greatly. Consequently, these wetted surface area changes were needed to be considered to estimate the resistance and effective power of the ship in full

scale. In the present study, the wetted surface area in running was estimated from the measured pitch and heave. Fig. 6 shows the variations of wetted surface area of the model ship according to the ship speed variations. Since the hull rose at high speed conditions, the wetted surface area decreased by approximately 40% at the design speed, by attaching spray rails.

Considering the wetted surface area variations, the residual resistance coefficient and the effective power of the ship in full scale were calculated and the results are shown in Fig. 7. The analysis was conducted according to the extrapolation method suggested by the International Towing Tank Conference (ITTC) (ITTC, 2014). The value of  $C_R$  was maximum at  $Fr_v$  of 1.247, which corresponds to 15 knots in full scale, and decreased in high speed conditions. Similar tendency of  $C_R$  was reported in the series of planing hull tests with increasing CG rise (Metcalf et al., 2005).

In the spray rails cases,  $C_R$  was larger than that in the bare hull case owing to greater rise of CG and smaller wetted surface area. Although there was difference in  $C_R$  among the spray rails cases, the effective power predicted for the hulls with spray rails at 8%  $T$  and 24%  $T$  was similar to that of the bare hull case. On the other hand, the effective power predicted for the hull with spray rails at 40%  $T$  was 21.4% larger than that of the bare hull case.

### 3.2. Seakeeping tests in head seas

Overall, spray rails (24%  $T$ ) installation produced reduced trim and hardly affect resistance performance. Seakeeping

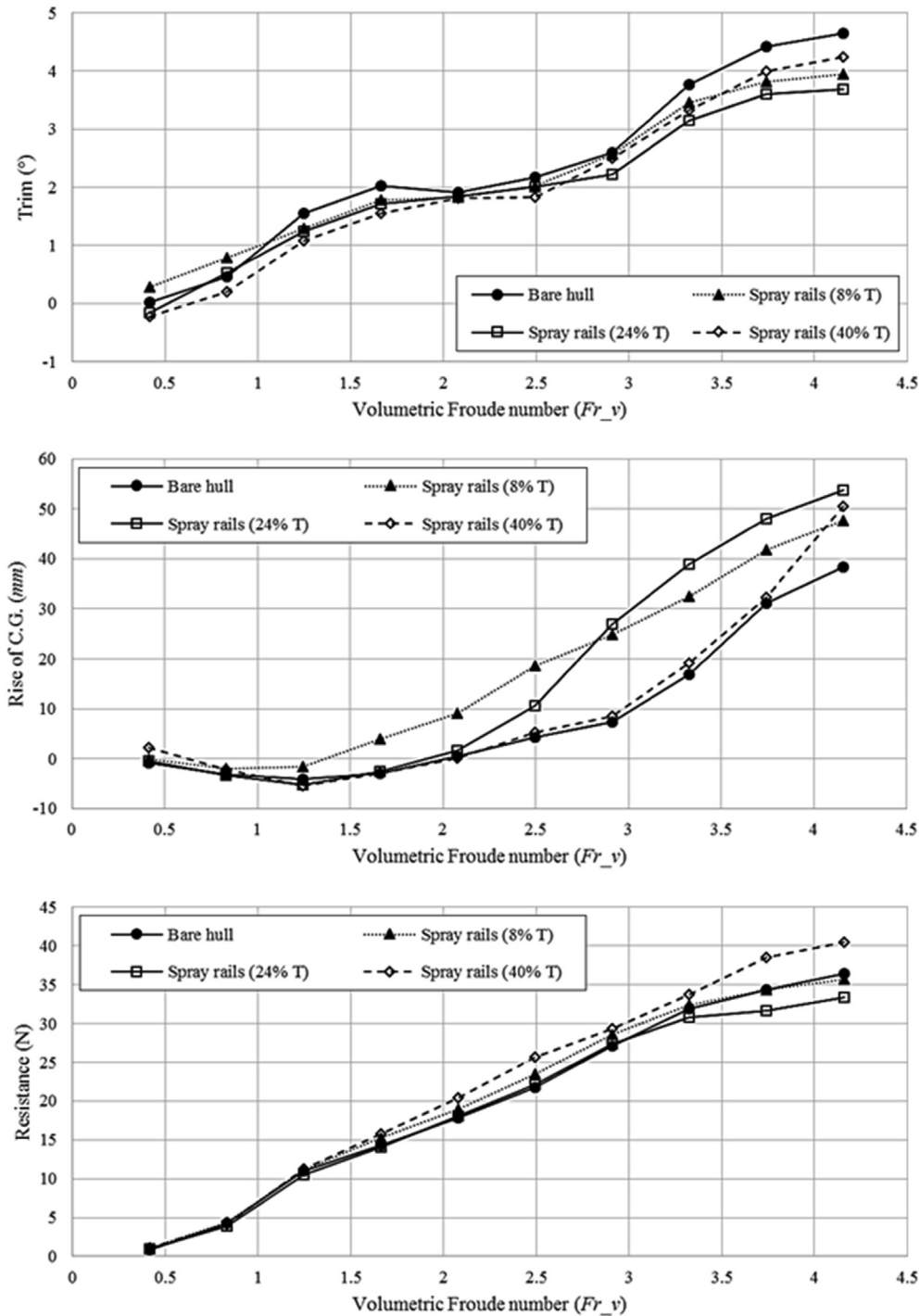


Fig. 5. Results of the resistance tests in calm water.

performance tests were conducted under the same condition and the results were compared with those for the bare hull. First, model tests were performed with and without spray rails at the optimal locations in head seas, which corresponds to 1 m wave height and 30 knots ship speed in full scale.

Fig. 8 shows the peak and trough values of the measured trim, rise of CG, and resistance in different wave conditions. In fully developed motion, five measurement peaks and trough values of the time history of motion and resistance

were selected and averaged to obtain the mean peak and trough value respectively; the differences between the mean peak and trough value of trim and rise of CG mean magnitude of pitch and heave motion respectively, which were used to derive the Response Amplitude Operator (RAO) of pitch and heave.

The magnitude of pitch and heave motion at  $\lambda/L_{PP} = 1.0$  was small, as the motion in waves was not developed in such a short wave condition. The difference rapidly increased at  $\lambda/L$

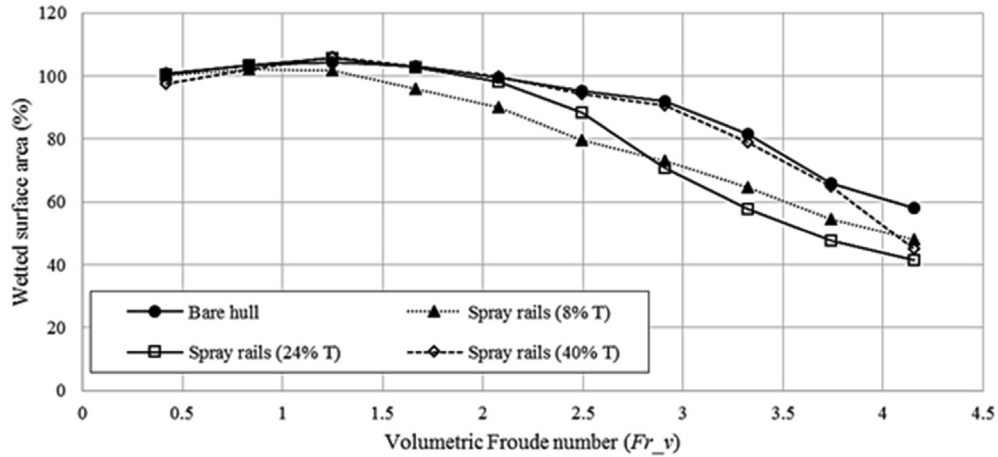


Fig. 6. Changes of the wetted surface area with the variation of the ship speed (wetted surface area at zero speed: 100%).

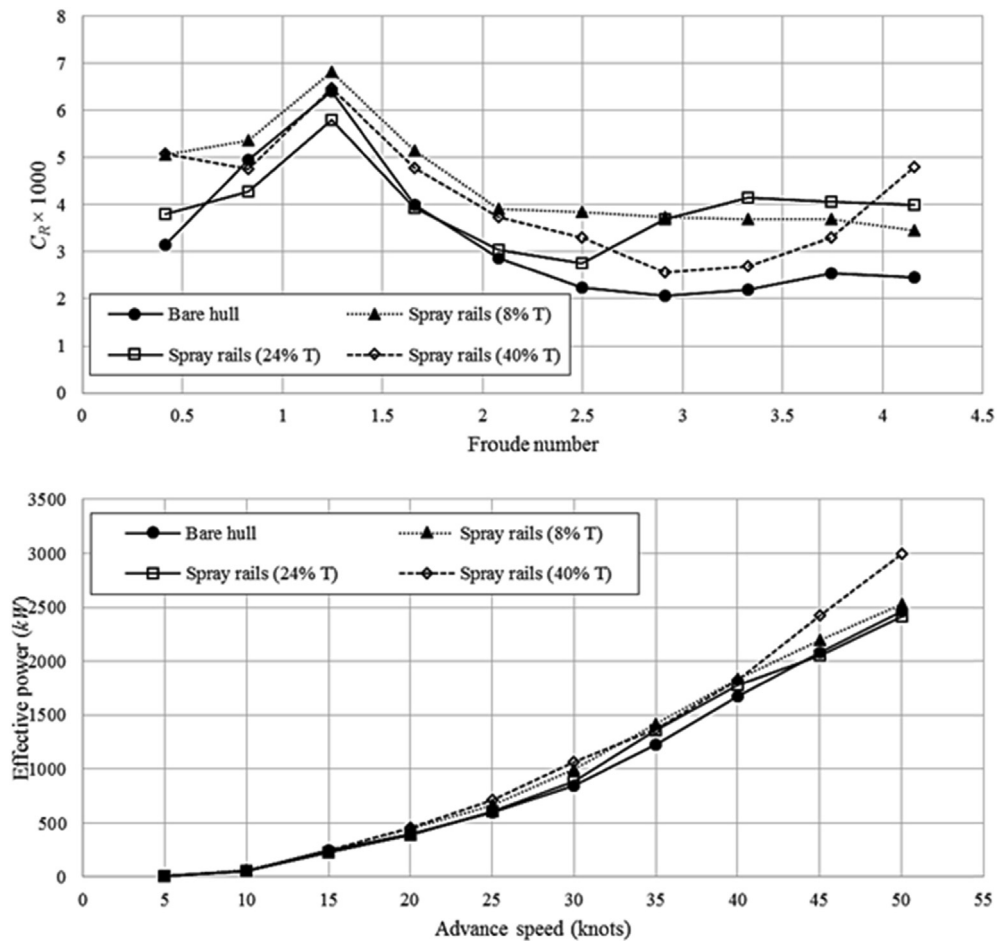


Fig. 7.  $C_R$  and effective power prediction of the wave piercing monohull in the full scale.

$L_{PP} = 2.0$ , as it was the resonance condition. Then the difference gradually decreased in long wave conditions. By applying spray rails, the peak and trough value of CG rise shifted to increase, similar to the calm water tests results. The peak resistance value decreased with increasing  $\lambda$ ; but the trough was found near 0 N regardless of the wave conditions.

RAOs of the pitch and heave motion were obtained from the measurement results. Fig. 9 shows the pitch and heave RAOs for the hull with and without the optimum rails case. The model test condition corresponds to 30 knots ship speed and 1 m wave height in full scale. The resonance, where the motion response rapidly increased, was observed when

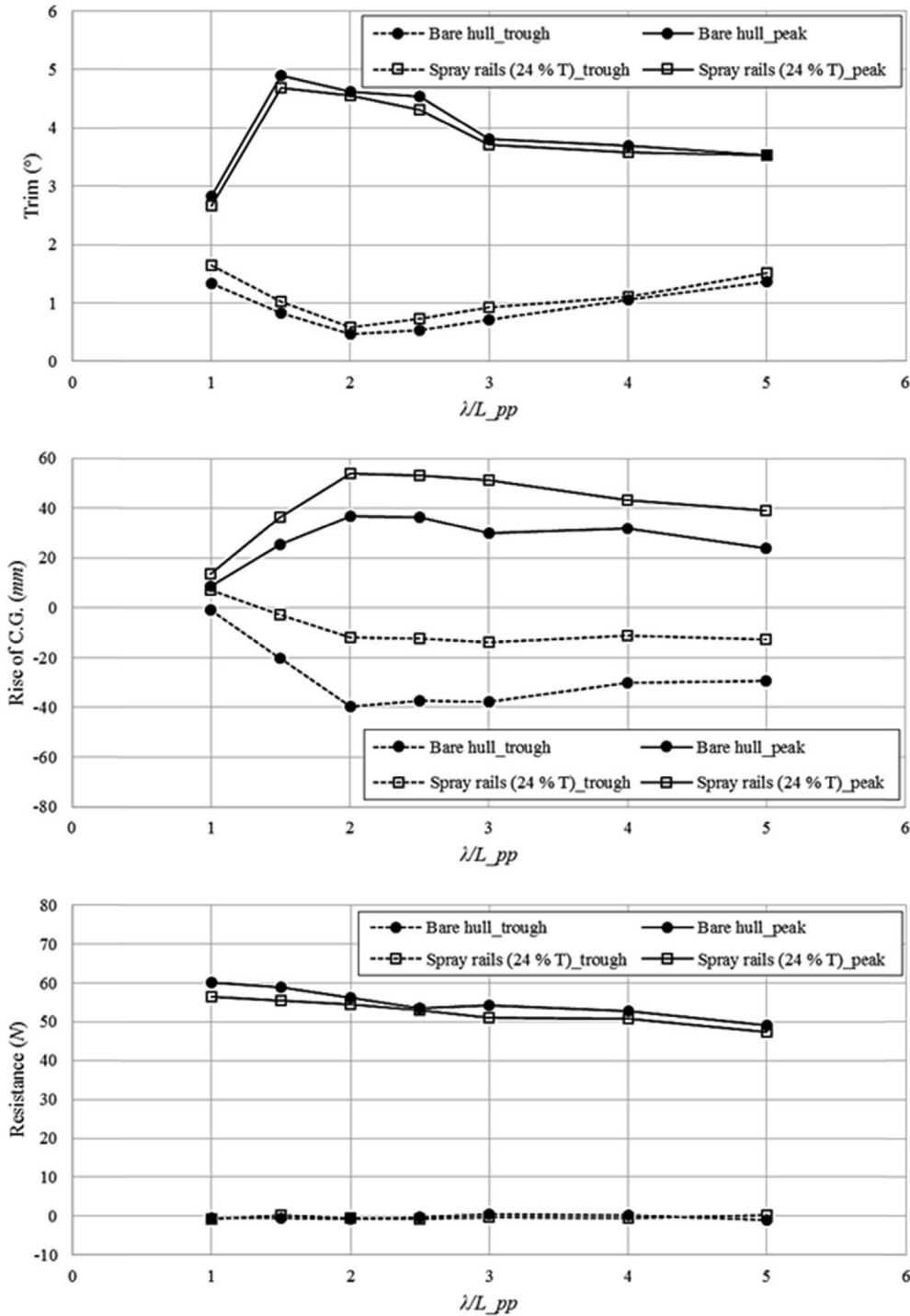


Fig. 8. Model test results in head seas (wave height 1 m, 30 knots).

$\lambda/L_{pp} = 2.5$  for the pitch motion and  $\lambda/L_{pp} = 2.0$  for the heave motion. When rails were attached on the hull, the pitch and heave RAO decreased under all wave length conditions. The pitch and heave RAO under resonance conditions decreased by 10.5% and 18.4%, respectively.

In Kim et al.'s study (2013), the pitch and heave motions were measured through model tests of a high-speed vessel and they were composed to obtain vertical displacement of the Fore Perpendicular (FP), considering the hull as a rigid body

with pitch and heave motion only. By second derivative of the vertical displacement, vertical acceleration of FP could be derived; however, the calculated vertical acceleration did not reflect the impact on the bow meeting the water surface that could be acquired from the direct measurement results by an accelerometer. Nevertheless, it could be used for qualitative assessment of the vertical acceleration of FP.

Fig. 10 shows the time-history of the heave and pitch measurement results and derived FP vertical displacement for

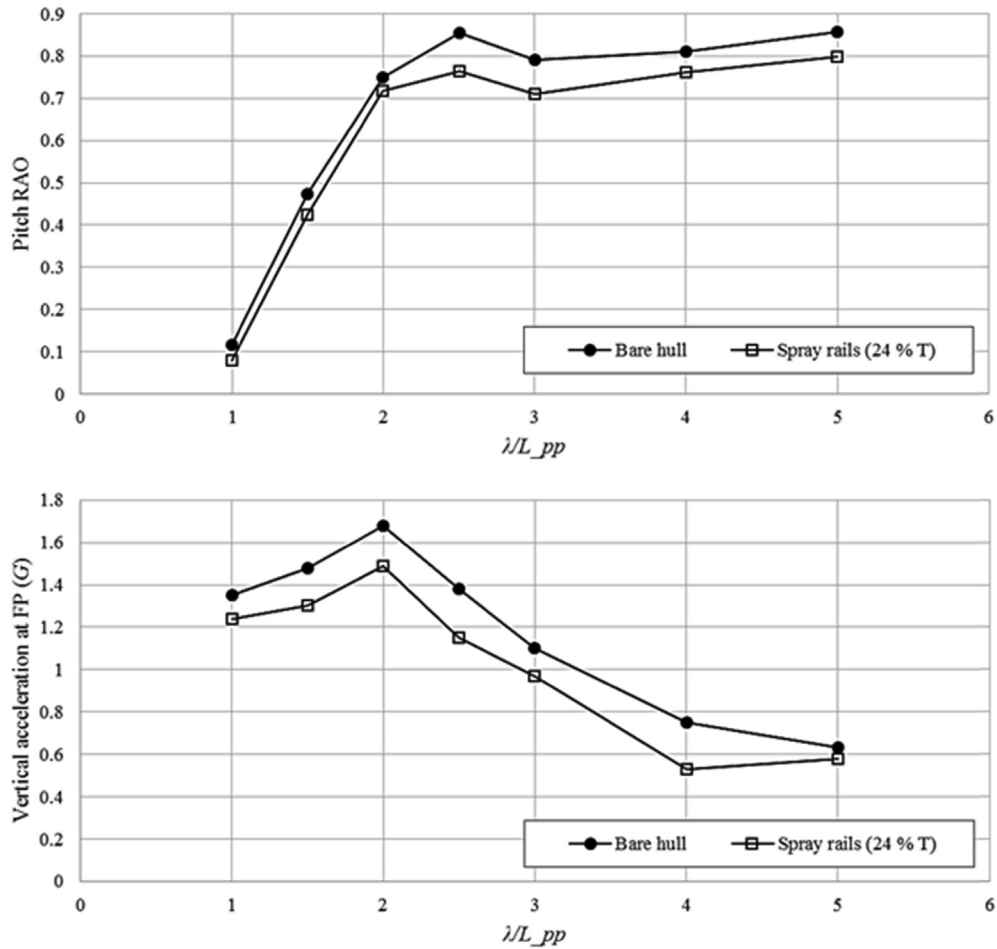


Fig. 9. RAO of pitch and heave motion (wave height 1 m, 30 knots).

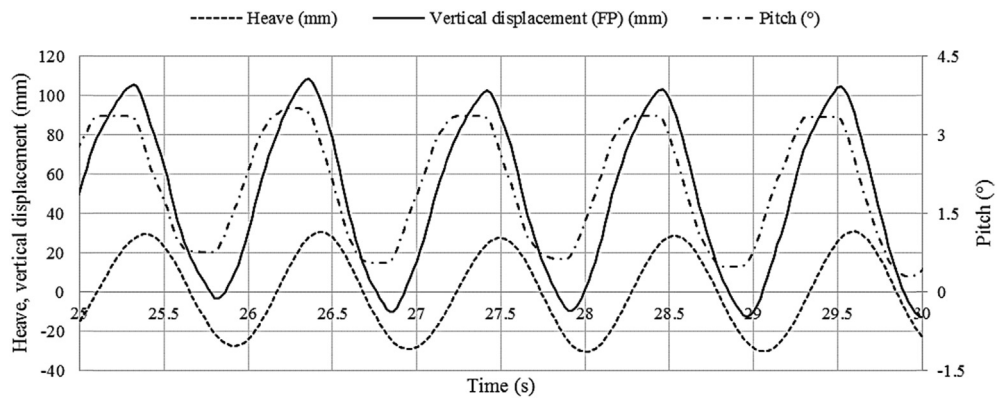


Fig. 10. Time-history of heave and pitch motion and vertical displacement of FP ( $\lambda/L_{pp} = 3.0$ , wave height: 1 m, advance speed: 30 knots).

$\lambda/L_{pp} = 3.0$ . The pitch and heave motions had a  $72^\circ$  phase lag. The FP vertical displacement was approximately two times that of the heave motion. In the time-history of pitch motion, clipped peaks and troughs were observed. As the hull has wave-piercing bow, the pitch motion was not developed immediately when the hull encounters wave; thus, the clipped peak and trough resulted in reducing vertical motion and acceleration of the bow in waves, which is the design principle of the wave-piercing bow.

Fig. 11 shows FP vertical acceleration obtained for the bare hull and optimum rails conditions. At the resonance condition ( $\lambda/L_{pp} = 2.0$ ), FP vertical acceleration decreased by 11.3% when the spray rails were attached on the hull. FP vertical accelerations were compared with the results of a planing hull in similar test condition (Fridsma, 1969). In the planing hull case, maximum FP vertical acceleration of the planing hull was larger than that of the wave-piercing hull in short wave conditions.

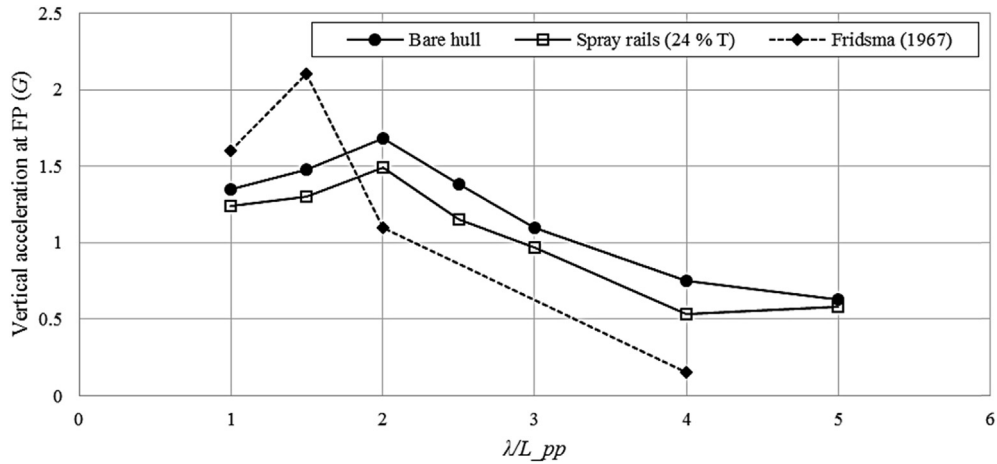


Fig. 11. Vertical acceleration at FP of the wave-piercing hull (wave height: 1 m, advance speed: 30 knots) and comparisons with a planing hull.

Effects of ship speed variations on the pitch and heave motion were also investigated by model tests in head seas. The model ship speed corresponded to 20, 30, and 40 knots in full scale. Furthermore, the wave height was also varied. In model tests, wave height of 0.0667 m, which corresponds to 1 m in the full scale, was applied in all  $\lambda/L_{PP}$  conditions first. Model

tests for wave height of 0.133 m, which corresponded to 2 m in the full scale, were conducted in long wave conditions, i.e.,  $\lambda/L_{PP} \geq 3.0$ , as the appropriate wave slope could be realized in such long wave conditions.

Fig. 12 shows the pitch and heave RAO results in difference ship speed and wave length conditions. For

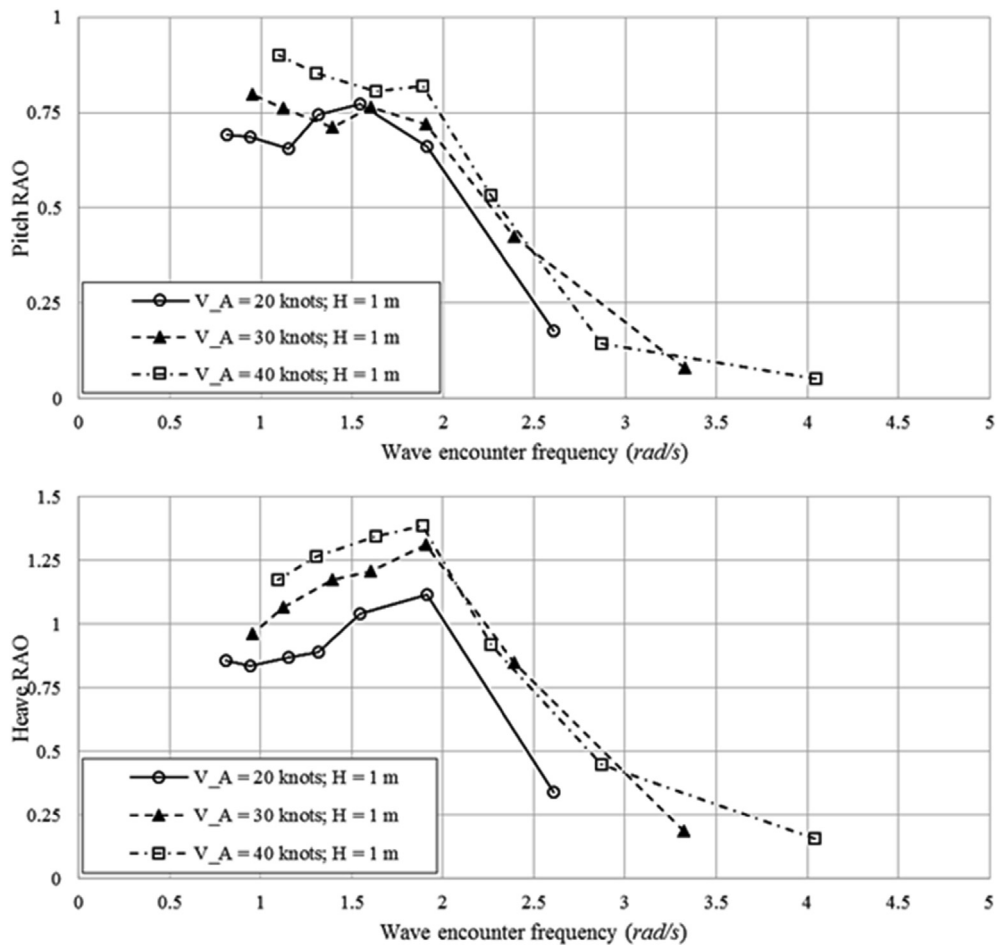


Fig. 12. RAO of pitch and heave motion: spray rails (24% T) case.

comparisons of the test results in different ship speeds, the wave-encounter frequency in the full scale was used, rather than the wave length ratio. For the heave RAO, the resonance region can be clearly observed near the wave-encounter frequency of 2 rad/s. In high wave-encounter frequency conditions, *i.e.*, short waves, the motion was not fully developed and RAO was small. In contrast, the RAO converged to 1 in the low frequency domain, as the test model followed the wave motion. The pitch RAO was small in high wave-encounter frequencies, similar to the heave RAO, but there was difference in the resonance frequency. In model speeds corresponding to 20 and 30 knots in full scale, resonance occurred around the wave-encounter frequency in full scale of 1.5 rad/s, whereas resonance occurred at 1.8 rad/s in 40 knots condition. It seems to be caused by the trim change in high speed. In high speed, as shown in the resistance test results, hull bottom was exposed and sea-keeping performance might change.

Fig. 13 shows snapshots of the model test conducted at  $\lambda/L_{PP} = 2.0$ . The bow was exposed above the water surface periodically, but the impact of slamming was expected to be smaller than that of conventional planing hull, as the bow of the test model has large deadrise angle and small bottom area.

Fig. 14 presents the comparison of estimated FP vertical accelerations with respect to the wave-encounter frequency. The largest vertical acceleration was found for the 40 knots condition, where the bow was frequently exposed above the water surface. For the 20 and 30 knots in full scale conditions, similar FP vertical acceleration was obtained whereas vertical acceleration of FP increased proportionally with the ship speed in the planing hull case (Fridsma, 1969).

The effective power in head seas was estimated using the average resistance obtained from the model tests and shown in Fig. 15. The effective power increased in the short wave region with a large wave-encounter frequency. The effective power also increased in high wave height cases.

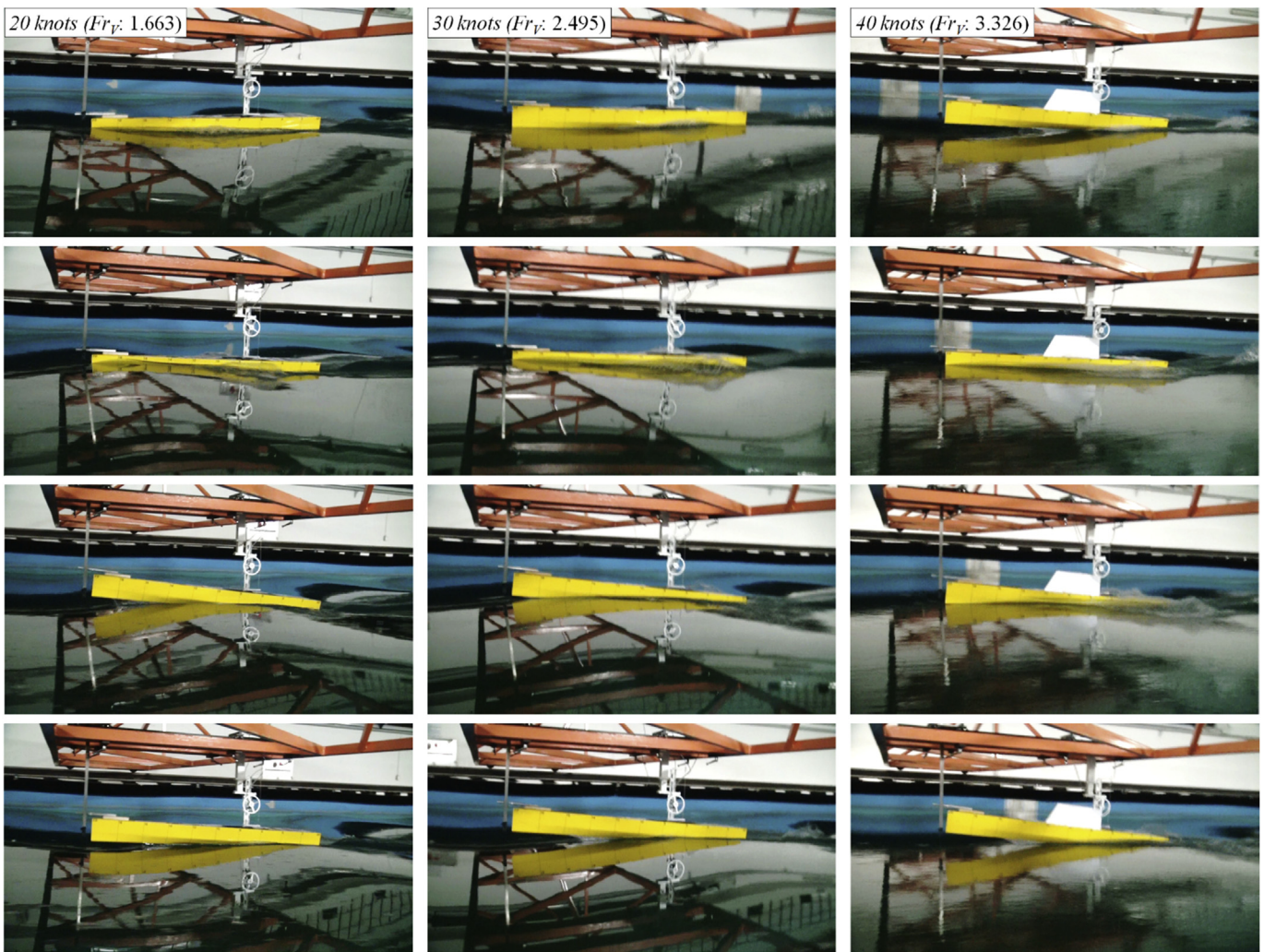


Fig. 13. Snapshots of the model tests in head seas (wave height: 1 m;  $\lambda/L_{PP} = 2.0$ ).

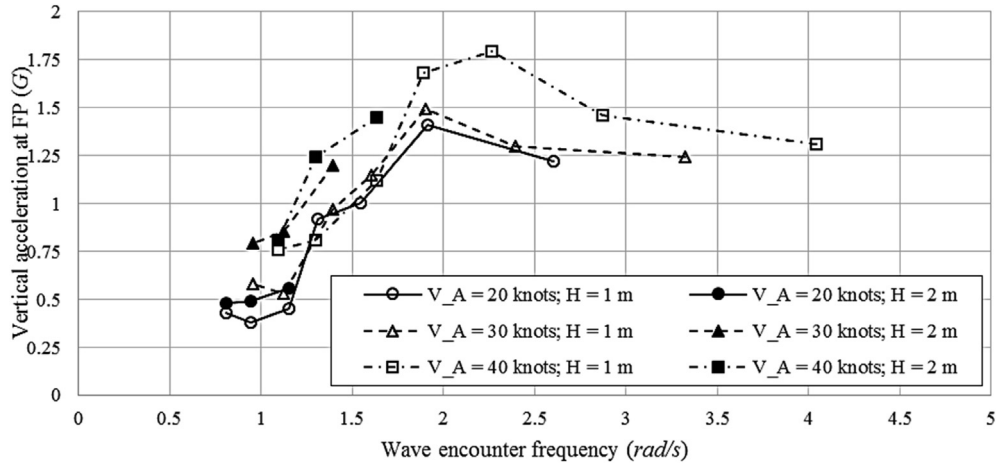


Fig. 14. Vertical acceleration at FP of the wave-piercing monohull with spray rails (24% T).

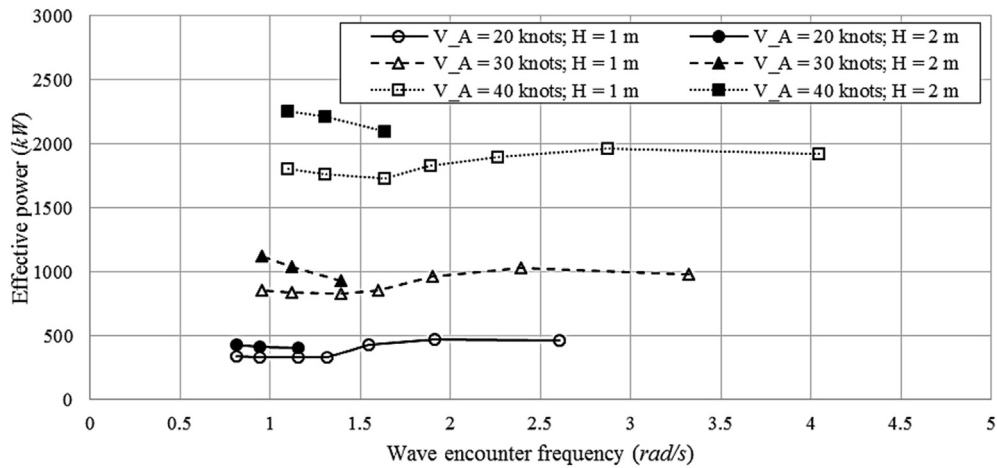


Fig. 15. Effective power prediction of the wave piercing monohull with rails in head seas.

#### 4. Conclusion and future work

The resistance and seakeeping performance of a newly-designed wave-piercing monohull were assessed through a series of model tests. Installing the wave-piercing bow and the spray rails reduced both the running trim and vertical acceleration of FP in waves. Resistance tests for the bare hull were conducted first, followed by tests of different locations of the rails in calm water. The trim of the bare hull in the design speed condition was 4.65°, and the rails at optimal location decreased the trim by approximately 0.97°.

The seakeeping tests were performed for the bare hull and the hull with the rails installed at the minimum running trim. It was revealed that the rails reduced pitch and heave motions of the hull in head seas. Pitch and heave both decreased, thus the FP vertical acceleration also diminished. Finally, the effective power of the ship in the full scale was estimated. The wetted surface area changes due to the trim and rise of CG variations in running were considered in the

extrapolation. The effective power increased in high wave-encounter frequency conditions.

In this study, the performed model tests focused on the resistance and seakeeping performance of the hull. As the hull has large  $L_{PP}/B$  and low transverse stability, its maneuverability is expected to be significantly different with that of conventional planing hull; research of the maneuvering of such hulls is needed to be pursued in the future study.

#### Acknowledgments

This research was supported by the IT R&D program of MOTIE/KEIT (Grant No. 100660329), the National Research Foundation grant funded by the Korean government (Grant Nos. 2013R1A1A2012597, 2011-0020563, and 2009-0083510), and Advanced Naval Vessel Research Laboratory funded by the Ministry of Defense. The support on experiments from Geuk-sang Yoo and Changhee Kim of Seoul National University is gratefully acknowledged.

## References

- ASME, 2005. Test uncertainty, The American society of mechanical engineers performance test code, No. 19.1-2005. American Society of Mechanical Engineers, New York, NY.
- Begovic, E., Bertorello, C., Pennino, S., 2014. Experimental seakeeping assessment of a warped planing hull model series. *Ocean. Eng.* 83, 1–15.
- Clement, E.P., 1964. Effects of Longitudinal Bottom Spray Strips on Planing Boat Resistance. *DTMB Report*, No. 1818. David Taylor Model Basin, Washington, DC.
- Fridsma, G., 1969. A Systematic Study of the Rough-water Performance of Planing Boats. *Davidson Laboratory Report*, No. 1275. Stevens Institute of Technology, Hoboken, NJ.
- Grigoropoulos, G.J., Chalkias, D.S., 2010. Hull-form optimization in calm and rough water. *Comput. aided Des.* 42, 977–984.
- Katayama, T., Fujimoto, M., Ikeda, Y., 2007. A study on transverse stability loss of planing craft at super high forward speed. *Int. Shipbuild. Prog.* 54 (4), 365–377.
- Keuning, A., Toxopeus, S., Pinkster, J., 2001. The effect of bowshape on the seakeeping performance of a fast monohull. In: *Proceedings of FAST Conference*, Southampton, 2001.
- Keuning, A., Pinkster, J., van Walree, F., 2002. Further investigation into the hydrodynamic performance of the AXE bow concept. In: *Proceedings of the 6th Symposium on High Speed Marine Vehicles*, Castello di Baia, Italy, 2002.
- Kim, D.J., 2012. A Study on the Running Attitude and Dynamic Stability of a Semi-displacement Round Bilge Vessel at High Speed. Ph.D. thesis. Seoul National University, Seoul, Korea.
- Kim, D.J., Kim, S.Y., You, Y.J., Rhee, K.P., Kim, S.H., Kim, Y.G., 2013. Design of high-speed planing hulls for the improvement of resistance and seakeeping performance. *Int. J. Nav. Archit. Ocean Eng.* 5, 161–177.
- Larsson, L., Eliasson, R.E., Orych, M., 2014. *Principles of Yacht Design*, fourth ed. Adlard Coles Nautical, London.
- Lavroff, J., Davis, M.R., Holloway, D.S., Thomas, G., 2013. Wave slamming loads on wave-piercer catamarans operating at high-speed determined by hydro-elastic segmented model experiments. *Mar. Struct.* 33, 120–142.
- Lewandowski, E.M., 1997. Transverse dynamic stability of planing craft. *Mar. Technol.* 34 (2), 109–118.
- Metcalf, B.J., Faul, L., Bumiller, E., Slutsky, J., 2005. Resistance Tests of a Systematic Series of U.S. Coast Guard Planing Hulls. *Report of Naval Surface Warfare Center Carderock Division*, No. NSWCCD-50-TR-2005/063. Naval Surface Warfare Center Carderock Division, Bethesda, MD.
- Sun, H., Faltinsen, O.M., 2011. Dynamic motions of planing vessels in head seas. *J. Mar. Sci. Technol.* 16, 168–180.
- Yousefi, R., Shafaghath, R., Shakeri, M., 2013. Hydrodynamic analysis techniques for high-speed planing hulls. *Appl. Ocean Res.* 42, 105–113.